Urban Climate 49 (2023) 101573

Contents lists available at ScienceDirect

Urban Climate

journal homepage: www.elsevier.com/locate/uclim

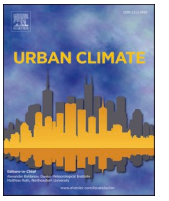

Rainfall-driven machine learning models for accurate flood inundation mapping in Karachi, Pakistan

Umair Rasool [a,b], Xinan Yin [a,*], Zongxue Xu [b], Roberta Padulano [c], Muhammad Awais Rasool [d], Muhammad Amir Siddique [e], Muhammad Azher Hassan [f], Venkatramanan Senapathi [g]

[a] State Key Laboratory of Water Environment Simulation, School of Environment, Beijing Normal University, No. 19 Xinjiekouwai Street, Beijing 100875, China
[b] College of Water Sciences, Beijing Normal University, Beijing Key Laboratory of Urban Hydrological Cycle and Sponge City Technology, Beijing 100875, China
[c] Regional Models and geo-Hydrological Impacts (REMHI) Division, Fondazione Centro Euro-Mediterraneo sui Cambiamenti Climatici, Via T.A. Edison, 81100 Caserta, Italy
[d] Department of Zoology, Wildlife and Fisheries, University of Agriculture, Faisalabad, Burewala Sub-campus, Punjab, Pakistan
[e] School of Architecture, Tianjin University, Tianjin 300072, China
[f] Tianjin Key Laboratory of Indoor Air Environmental Quality Control, School of Environmental Science and Engineering, Tianjin University, Tianjin 300072, China
[g] Department of Disaster Management, Alagappa University, Kariakudi 630003, Tamil Nadu, India

ARTICLE INFO

Keywords:
Rainfall amount
Urban pluvial flooding
Machine learning models
Flood inundation mapping

ABSTRACT

Urban pluvial flooding (UPF) has emerged as a serious natural hazard, especially in recent years. Previous research on UPF prediction has mainly focused on hydrological models, which required a large amount of data. However, a data-driven method can significantly reduce the computational cost by using rainfall amounts to predict pluvial flooding. Intensity-duration-frequency (IDF) curves using the Gumbel method can provide a better interpretation of the correlation between rainfall intensity, duration, and probability of occurrence of a given rainfall amount. In this study, machine learning models (ML) for rainfall amounts were used to identify flood points in a case study conducted in Karachi, Pakistan. Thirteen inundation factors were used for the ML models, including a new factor, curve number. Ten ML models were applied first on training and then on validation data, yielding the inundation points. The training and validation process of the model included 384 flood points. Several statistics were used to verify the performance and accuracy of the model. We found that the Light Gradient Boost Machine and Random Forest Classifier models were the most accurate in training and validating the model, while the Decision Tree and K-Nearest Neighbor models were the least accurate in training and validating the model. The study provides valuable information for decision makers to protect communities from flood hazards by incorporating the likely intensity and duration of rainfall events and carefully selecting influencing factors into flood event prediction models.

* Corresponding author.
E-mail address: yinxinan@bnu.edu.cn (X. Yin).

https://doi.org/10.1016/j.uclim.2023.101573
Received 2 April 2023; Received in revised form 12 May 2023; Accepted 31 May 2023
Available online 10 June 2023

1. Introduction

Urban pluvial flooding (UPF) is a flow of water that occurs when runoff exceeds the capacity of the drainage system, this can occur either when the water flows into the system or when it is discharged (Azizi et al., 2022). The occurrence of UPF in urban areas, caused by short-duration, high-intensity rainfall events, is a persistent issue that leads to property damage and disruption in cities worldwide (Sandink and Robinson, 2022). The UPF is driven by many local factors, such as the type and nature of impermeable surfaces in the basin, maintenance of sewage and manhole, underground structures, and extensive growth of urbanization (Agonafir, 2022; Darabi et al., 2019). The threat of UPF to numerous cities worldwide has grown in recent years (Ke et al., 2020; Netzel et al., 2021). Moreover, with the projected increase in intensity and frequency of storm events due to climate change, the risk of UPF is expected to further escalate in the future (Ohba and Sugimoto, 2019). City authorities need to forecast extreme precipitation events to avoid UPF and its impacts. Accurate precipitation forecasting requires correct predictions of peak intensity, duration, and timing of arrival, which typically requires extensive modeling resources. In contrast, a rapid and efficient approach can involve the utilization of machine learning (ML) models based on a rainfall threshold. By comparing the current or predicted precipitation levels with the threshold, it becomes easy to estimate the likelihood of flooding in the town (Wu et al., 2023; Yang et al., 2016).

Rainfall patterns are critical to hydrologic science, flood forecasting, modeling, and drainage design (Sangati and Borga, 2009). The impact of urbanization on climate change and meteorological hazards has attracted global attention (Sathish et al., 2022) due to the frequency and intensity of extreme weather events (Marelle et al., 2020), such as heavy rainfall, leading to devastating hazards like flooding (Mondal et al., 2022). Recent studies have focused primarily on spatiotemporal patterns (Kron et al., 2019), influencing factors (Bruwier et al., 2020), flood vulnerability (Choubin et al., 2019) and risk assessment (Thanh Son et al., 2022). Urbanization is changing the pattern and intensity of rainfall, mainly due to anthropogenic warming and greenhouse gas emissions (Zou and Ren, 2015). In South Asian region, the increase in temperature and monsoon season leads to increased flood frequency (Das et al., 2021), especially in fast-growing urban areas located on riverbanks without proper planning, which further aggravates the situation (Pervin et al., 2020). In Beijing, urbanization results in a substantial increase in heavy and moderate rainfall events, while light rainfall remains unaffected (Yu et al., 2020). The main reason for severe flooding every year in Mumbai city, as well as other cities in India, is attributed to the increasing amount of rainfall (Naikoo et al., 2022). Another study conducted on Dhaka city where 56 years (1953–2009) rainfall

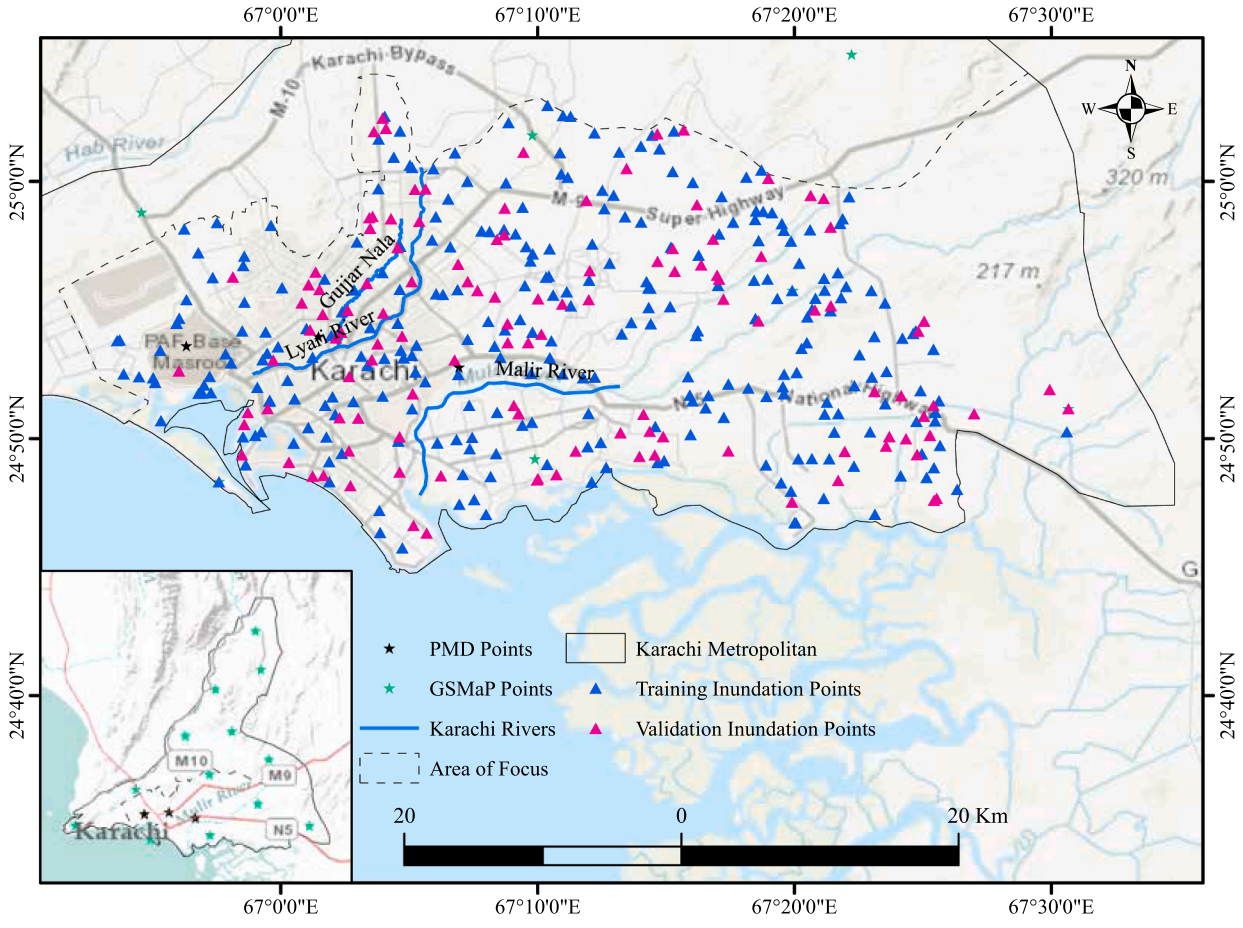

Fig. 1. Location and inundation points of the study area.

data revealed extreme events with a 100-year return period, and forecasted annual rainfall over 200 mm in any 12-year period from 2010 to 2066 (Ahammed et al., 2014).

ML is a family of statistical and computer-based algorithms that train numerical models to predict decisions based on observed samples. ML and other Deep learning methods are being effectively used in water resource management such as flood prediction (Mosavi et al., 2018), water quality analysis (Asadollah et al., 2021), and sediment transport (Abeshu et al., 2022), particularly in urban hydrology where physics-based models face high uncertainties and complexity (Mehedi et al., 2022). In hydrology/hydraulics, ML is meant to explore the relationship between water and human systems to provide effective design and management instruments (Shen et al., 2018). For example, the highly accurate evaluation of flood-prone areas by ML modeling could aid in developing flood-defense plans in river basins, as well as flood and flash-flood early warning systems (Brillinger et al., 2020). Although ML algorithms have demonstrated their effectivity in flood prediction and forecasting (Mosavi et al., 2018; Tayfur et al., 2018) in the absence of drainage data, flood inundation, and high-resolution topography, only a few studies exist which utilized ML to categorize or predict UPF, which makes it a challenging issue. (Yang et al., 2016). ML models can digitally replicate flood non-linearity without physical process information, based on historical flood data (Ahmad et al., 2022; Mosavi et al., 2018). The usage of these modern ML models assures high-precision results. ML models also incorporate specific strategies for testing outputs and evaluating the models' performance (Xue et al., 2022).

In recent years, Pakistan has faced record-breaking rainfall in Sindh, Khyber Pakhtunkhwa (KPK), and Punjab. As major floods swept through Sindh Province due to monsoon rains, at least 1.7 million acres of arable land were flooded in September 2011. In 2003, Karachi experienced UPF, with 284.5 mm of recorded rainfall in two days. In 2007, Monsoon precipitation severely affected the KPK, Sindh, and coastal Baluchistan. In August 2020, the heaviest rain in Karachi recorded 231 mm in just 12 h and 484 mm on a single day in its history, breaking 90 years of rainfall record history in a single day. Therefore, we selected Karachi as the present case study area, which frequently experienced floods in the past decade. Our study presents a novel approach to urban flood prediction using machine learning and a data-driven methodology. We used thirteen flood conditioning factors, including a new conditioning factor - curve number - and used several statistical measures to test the accuracy of the models. Our approach makes a valuable contribution to UPF prediction by incorporating new elements that improve the accuracy of flood prediction models. The specific objectives of the present study include (a) evaluating the various conditioning factors to determine their importance for UPF, (b) applying ML models to historical rainfall data to identify flooded areas, and (c) evaluating the performance of ML models and their advantages and disadvantages during the modeling process.

2. Case study and data description

2.1. Study area description

Karachi is a densly populated port city in Pakistan with tropical climate, covering 3527 km^2 urban area, located along the Arabian Sea coast (Fig. 1) that contains semi mountaneous flat landscape on its western and northern borders. The city's population is concentrated along the southern and southeast banks of the Malir river (City District Government Karachi, C, 2007). Karachi has a population of over 16 million people with 4115 people per km^2 (Ahmed et al., 2008) and expected growth of over 20 million by 2025 (Statistics, P. B. O, 2017). The study area is facing unplanned urban growth, insufficient access to basic infrastructure, problems with solid waste management, crowded public transportation, environmental degradation, and bad governance (Bank, W, 2018), where nearly 40% of the population lives in slums (Haq, 2014; Hasan et al., 2013). The region has a tropical climate with warm winters and hot summers, characterized by an average minimum temperature of 13 °C during winter and an average maximum temperature of 34

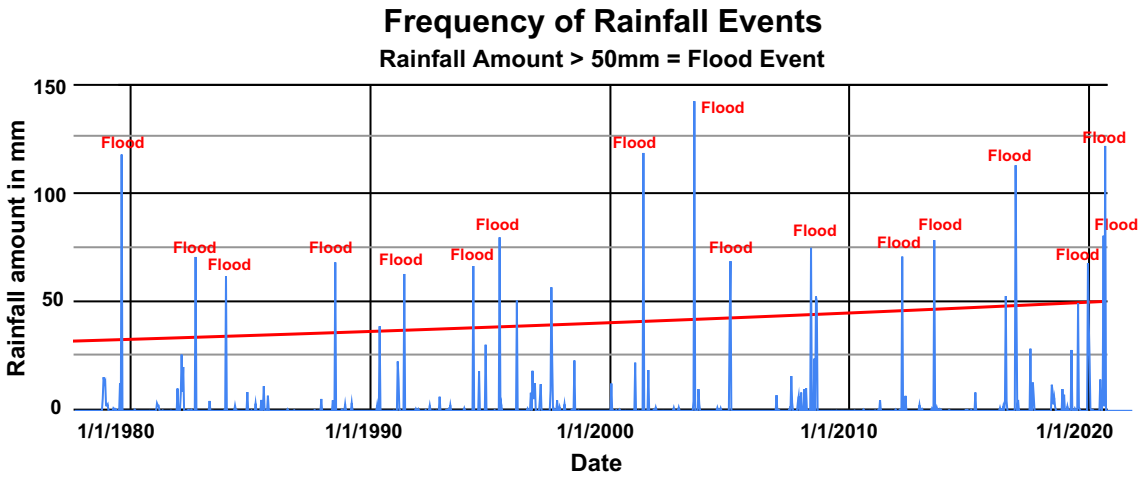

Fig. 2. Historical rainfall and associated urban pluvial flood events between 1979 and 2020.

°C during summer while the precipitation is limited, with an average annual rainfall of just 200 mm (Wu et al., 2022).

Due to unplanned development and poor urban management, city's rivers are seriously affected. The Malir River basin primarily consisted of a large network of streams, but rapid urban development and encroachment resulted in many stream abatements. Localized flooding after intense rains, an increase in impermeable land cover (which increases surface overflow rates), and congestion, are some of the effects on surface hydrological processes and Karachi's current most significant problems (Bakhsh et al., 2011). Climate change driven increased intensity and frequency of rainfall further burdens the city's poor drainage system (Mirza, 2003). In Karachi, three types of drainage encroachments are typically observed: (a) upscale house projects that encroach near sea outfalls, (b) illegal settlements (slums) that encroach on natural drainage, and (c) development schemes that encroach on natural drainage channels, substantially reducing their width. The decreased drainage capacity, changes in hydrological and hydraulic processes, and resultant floods in urban areas are primarily caused by the inadequate capability of the sanitary system and encroachments in river or channel beds and these factors play a critical role in the problem faced by urban areas. (Fernández and Lutz, 2010).

2.2. Rainfall observations

The 42 years (1979–2020) daily rainfall intensity data were acquired from 3 ground-based rainfall gauges installed by the Pakistan Meteorological Department (https://www.pmd.gov.pk/en/) to find out the actual time and amount of rainfall that triggered UPF. According to the primary data: (i) irrespective of rainfall duration, all the flood events occurred with rainfall amounts of at least 50 mm within 3 h, (ii) rainfall amount increased with time (1979–2020), and (iii) frequency of UPF almost doubled in recent two decades (12 events) compared to prior two decades (7 events), as shown in Fig. 2.

Due to the limited number of rain gauges available for an area of 3527 km^2, this study required rainfall data from multiple sites. Only three rain gauges were found to be insufficient for this purpose. To address this issue, the study employed Global Satellite Mapping of Precipitation (GSMaP) data developed by the Japanese Precipitation Measuring Mission (PMM)(Mega et al., 2018). This technology is capable of producing a global precipitation map with high precision and resolution by utilizing data from multiple PMW/IR sensors carried by different satellites (Chen et al., 2019b). The algorithm fills gaps between estimates using cloud motion vectors and modifies precipitation rates with a Kalman filter model (Ushio et al., 2009). To minimize latency, the GSMaP_NRT product was

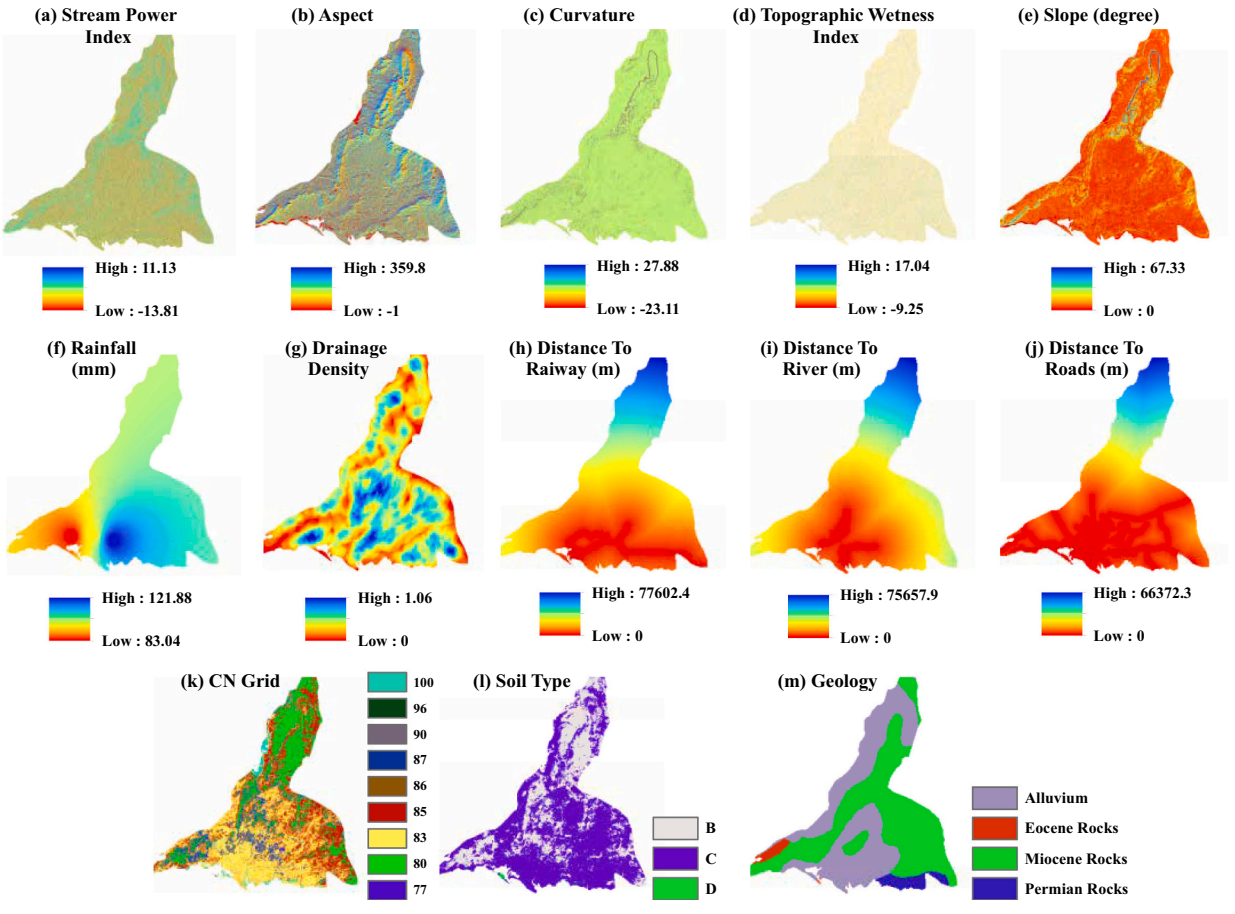

Fig. 3. Conditioning factors used in this study relevant to UPF.

developed for near real-time operation using forward cloud movement. For this study, GSMaP_NRT products were selected, and rainfall data were downloaded from 13 different locations.

For this study, hourly precipitation data from GsMap were converted to daily precipitation data. The process of converting hourly data to daily data involves several steps. First, the hourly data are grouped into daily intervals, which is usually done by summing the values for each day. Second, the daily average is calculated by dividing the summed values by the number of hours in a day. This step ensures that the daily values are representative of actual daily conditions. Finally, the daily data were exported to an appropriate format, such as a CSV format, to allow for further analysis and visualization.

2.3. Flood conditioning factors

UPF can cause significant damage, emphasizing the need for effective flood risk analysis criteria. To develop these criteria, the study used a Shuttle Radar Topographic Mission (SRTM) 30-m digital elevation model (DEM) to extract several morphometric explanatory factors, including Topographic Wetness Index (TWI), altitude, slope in degrees, drainage density, Stream Power Index (SPI), aspect, and surface curvature. This study utilized rainfall as the dependent variable and 13 conditioning factors as explanatory factors. The conditioning factors were selected based on their relevance to UPF, and their spatial distribution was determined based on exposure values. The conditioning factors included land use, geology, distance to roads, distance to the railway, distance to the river, soil cover type, Soil Conservation Service Curve Number (SCS-CN), drainage density, TWI, aspect, slope, SPI, and surface curvature as shown in Fig. 3. These conditioning factors have been discussed in detail by previous researchers (Bouramtane et al., 2021; Costache et al., 2021; Islam et al., 2021; Mirzaei et al., 2021a; Yuan et al., 2021).

We have introduced one important conditioning factor in the UPF risk analysis previously neglected: the SCS-CN, developed by the Soil Conservation Service of the United States in 1954, which is used to calculate the direct runoff depth from storm rainfall depth (Ling et al., 2020). The CN is a function of a watershed's land use/cover, soil permeability, geology, and other runoff-producing factors; in the SCS-CN method, it is used to estimate direct runoff only relying on cumulative rainfall depth (Hawkins et al., 2019).

2.4. On-ground validation of UPF points

We utilized data from the Pakistan disaster management authority (PDMA), PDMA-Sindh, social media reports (i.e., Twitter, Facebook), and mainstream print and electronic media (Bhatti, 2021; HANDS, 2020) to compile recent four years of UPF events that consisted of 384 inundation points in the study area. The information collected was then reviewed and analyzed to ensure its accuracy and consistency. Inconsistencies and discrepancies in the data were resolved through careful review and analysis. We found that the majority of the pluvial flood events occurred between July and September each year during the monsoon. We considered only those pluvial flood inundation areas where the water depth was 300 mm during the floods because this depth may not immediately threaten life but may cause economic loss. The methodology used in this study highlighted the importance of a multi-faceted approach to data collection and analysis in developing a comprehensive understanding of flood situations. Table 1 provides an overview of the data used in this study.

3. Methods description

3.1. Mapping rainfall distribution in flood-affected regions

This study was designed to determine the relationship between precipitation amount and the occurrence of UPF in a specific study area. Precipitation data were collected from 13 different locations and ArcGIS-based 'inverse distance weighting' (IDW) interpolation technique was used to create a continuous spatial representation of precipitation distribution in the study area. Analysis of the precipitation data indicated that pluvial flood events are most likely to occur when precipitation exceeds 50 mm within a 3-h period. A binary system was used to classify flood points, with 0 representing areas with $<$50 mm of precipitation and 1 representing areas with $>$50 mm of precipitation (Bhatti, 2021; HANDS, 2020). This approach provided a scientific basis for analyzing the relationship between precipitation and UPF occurrence, which can serve as a basis for flood risk management and mitigation strategies in the study area.

Table 1
Detail description of the dataset used in this study.

Data type	Source	Scale	Time period
Flood Inundation Data	Published reports; social media and print media	Randomly selected	2017–2020
Rainfall data	Pakistan Meteorological Department	Daily data	1979–2020
GSMaP data	Japanese Precipitation Measuring Mission	Hourly	2017–2020
Geology	Geological Survey of Pakistan	1:250,000	2011
DEM data	SRTM, USGS Earth Explorer website	1 arc *sec*	2014
Soil data	FAO Soil	1:5000000	_
Topographical data	Survey of Pakistan	_	_
Satellite image	Sentinel 2, USGS Earth Explorer website	10 spatial resolutions	6/12/2020

3.2. Method to extract data from conditioning factors

From the SRTM DEM, six morphometric factors were derived with a spatial resolution of 30 × 30 m, including TWI, slope, aspect, drainage density, and SPI. Additionally, the distances to the railway, road, and river were generated with the Euclidean Distance tool within the spatial analysis feature of ArcGIS. The geologic map was created using the geologic toposheet. Google Earth Engine platform was utilized to create a land use map using Sentinel-2 data with 10 m spatial resolution (Benhammou et al., 2022). The soil map of the study area was taken from the FAO website (https://www.fao.org/). Munna et al. (2021) calculations were utilized to extract the raster values of SCS-CN from the land use classes and soil data.

The conditioning factors with high resolution were resampled to 30 m resolution using the "resample tool" in ArcGIS. The values were then extracted over the flooded and non-flooded points using the "extract multi values to points" tool. The collected point values were imported into google collab for further modeling.

3.3. Multi-collinearity analysis

A multi-collinearity test was performed to ensure that the regression assumptions in this study were correct (Yin et al., 2023). The variance inflation factor (VIF) method is widely used in the feature technique to select appropriate features and reduce redundancy for prediction (Abood and Salman, 2021). The VIF is typically used to diagnose multi-collinearity among independent variables prior to regression (Stine, 1995). The coefficient of determination (R^2) is used to calculate the VIF, a VIF value of $\leq$10 indicates that there is no significant collinearity (Huang et al., 2023). The VIF values for all factors were <2.5, indicating that all independent variables were free from multi-collinearity problems. In addition, the tolerance criterion indicated satisfactory results with values of >1, confirming the suitability of all selected factors for further analysis (Mehravar et al., 2023). Table 2 provides the VIF and tolerance values of all parameters used for this study.

3.4. Frequency distribution and the development of IDF curves

The study examined the relationship between precipitation intensity, duration, and frequency (IDF) over a period of 42 years. To interpret the results, Gumbel distribution model was utilized, which is commonly used for flood probability analysis and modeling extreme weather events. The relationship between intensity, duration, and frequency (IDF) of precipitation data over 42 years was analyzed and interpreted using the Gumbel distribution, a widely used model for flood probability analysis and other extreme weather events modeling (Kareem et al., 2022). According to Elsebaie (2012), the Gumbel approach is easy to implement and can be used for extreme events such as rainfall peaks. The precipitation frequency P_T (in mm) for each duration is calculated considering the specified return period T (in years).

$$P_T = P_{ave} + K \times S \tag{1}$$

The term P_{ave} refers to the average annual maximum precipitation depth or amount that can be obtained during a given period, term P_i is the rainfall individual extreme value, and n is the recorded number of years or events and calculated as follows:

$$P_{ave} = \frac{1}{n}\sum_{i=n}^{n} P_i \tag{2}$$

K is the Gumbel frequency factor where T is the return period, and ln is the natural logarithm, which can be calculated as follows:

$$K = -\frac{\sqrt{6}}{\pi}\left[0.577 + ln\left[ln\left(\frac{T}{T-1}\right)\right]\right] \tag{3}$$

The standard deviation or S is calculated by the following equation where P_i is the rainfall individual extreme value, P_{ave} is the

Table 2
VIF and tolerance values of the parameters used for this study indicating no multi-collinearity between the factors.

Factors	VIF	Tolerance
Geology	1.797	0.557
SPI	2.189	0.457
D. to Roads	1.510	0.662
D. to Railway	1.258	0.795
D. to River	2.196	0.455
TWI	1.412	0.708
Drainage	1.221	0.819
Curvature	1.711	0.584
Aspect	1.045	0.957
CNGrid	1.121	0.892
Slope	1.217	0.822
Soil	1.125	0.889

average annual maximum precipitation depth, and n is the recorded number of years or events.

$$S = \left[\frac{1}{n-1}\sum_{i=n}^{n}(P_i - P_{ave})^2\right]^{½} \quad (4)$$

The rainfall intensity, I (mm/h) for the return period T is calculated from:

$$I_t = \frac{P_T}{T_d} \quad (5)$$

where PT is the precipitation frequency for a given duration and return period, and Td is the duration in hours.

3.5. Feature selection and machine learning models

The term "feature selection" refers to a group of techniques for assigning values to input features in a predictive model, specifying the relative significance of the factors during the prediction. It plays a significant role in ML models. Three feature selection algorithms are present in the literature: Correlation-based feature selection (Hall and Smith, 1999), Relief-F (Urbanowicz et al., 2018), and the Extra Trees Classifier ensemble method (ETC) (Drover et al., 2017). For the present work, we selected ETC for feature selection and ranking based on their importance. ETC is an ensemble method that applies averaging to reduce over-fitting caused by randomized decision trees on different subsamples of the dataset and boost forecast accuracy (Ceballos, 2019). Then, each feature is ranked according to its significance, and the best features can be chosen.

ML models refer to a collection of algorithmic methodologies that heavily rely on data. These techniques are distinct from traditional statistical methods as they do not rely on a pre-determined equation as the core model. Instead, ML models rely on specific algorithms to train a model using available data, and then apply this model to new, unseen data. Importantly, the performance of ML algorithms typically improves as the volume and quality of training data increase. There are two broad categories of ML algorithms: supervised and unsupervised learning. Supervised learning algorithms aim to identify functions that can map inputs to labeled outputs, within supervised learning, there are further subdivisions into regression and classification methods, depending on the nature of the output variable. Unsupervised learning, on the other hand, attempts to identify patterns or structure in the data without pre-existing labels or outcomes. The unsupervised learning is commonly used for clustering or dimensionality reduction (Ke et al., 2020). Classification is a common technique used to predict floods (Tayfur et al., 2018), which involves distinguishing flood events from non-flood events by analyzing hydrological variables and utilizing prior knowledge of past flood and non-flood occurrences.

The dataset was randomly divided into training and testing for the present study by a 70:30 ratio, and 10 different ML models were applied: Decision Tree (DT), Random Forest (RF), LoGistic regression (LG), Neural Networks (NNs), Support Vector Machine (SVM), eXtreme Gradient Boost (XGBoost), K-Nearest Neighbor (KNN), Naive Bayes (NB), Light Gradient Boosting Machine (LightGBM) and Cat Boost Classifier (CBC). A brief introduction to these algorithms is described below.

3.5.1. Decision tree (DT)

DT constructs a top-down tree-like structure from the roof to the leaf nodes (Breiman et al., 2017). Separate subsets of the data are identified using a prediction rule, i.e., population subgroups are identified hierarchically by a series of binary partitions of the model's anticipated data (Venkatasubramaniam et al., 2017). To run this model, the "DecisionTree" classifier was used in the Jupyter notebook.

3.5.2. Random forest (RF)

RF is another powerful and effective machine-learning algorithm, developed to promote skill prediction by extending the concept of regression and classification trees (Razavi-Termeh et al., 2019). This algorithm has a lower computational burden, better performance in high-dimensional feature space, and allows measuring the importance of input variables for a better understanding of their contribution to overall classification accuracy (Rodriguez-Galiano et al., 2012). To run the model, the "randomforest" classifier was used in the Jupyter notebook.

3.5.3. LoGistic regression (LG)

It is a statistical model which describes the correlation between the probability of a binary variable and a collection of associated explanatory factors (Bouramtane et al., 2021). The logistic regression model is constructed by optimizing the regression coefficients and used to estimate the chance of the occurrence of an UPF (value = 1) or not (value = 0) in this study. To run the model, the "LogesticRegression" classifier was used in the Jupyter notebook.

3.5.4. Neural networks (NN's)

NNs can construct complex features using simplified representations created by previous layers (Goodfellow et al., 2016). They can also use a smaller amount of training data to improve results compared to other methods (Kim et al., 2018). To run the model, the "MLP" classifier was used in the Jupyter notebook.

3.5.5. Support vector machine (SVM)

SVM is a supervised ML method based on the fundamental risk minimization rules and mathematical theory (Tehrany et al., 2015). The SVM model is known for its quick layer recognition and analysis, as stated by (Micheletti et al., 2011). This model is often employed to address classification and regression problems while minimizing overfitting of the algorithm (Gayen et al., 2019). To run the model, the "svm" classifier was used in the Jupyter notebook.

3.5.6. eXtreme gradient boost (XGBoost)

The fundamental principle of this technique is to construct a new foundation that is highly correlated with the ensemble's subsequent negative gradient of the loss function (Natekin and Knoll, 2013). The Boosting algorithms are relatively simple to execute, permitting experimentation with several model designs. Furthermore, they exhibited significant success in a variety of ML and data-mining tasks, in addition to practical applications (Hutchinson et al., 2011; Pittman and Brown, 2011). To run the model, the "XGB" classifier was used in the Jupyter notebook.

3.5.7. K-nearest neighbor (KNN)

KNN is a distance-based learning strategy that evaluates the major class of the k-closest points to estimate the projected response of a given point (Cover and Hart, 1967). The KNN algorithm is a simple and intuitive learning technique generally utilized in various applications (Cheng et al., 2014). To run the model, the "KNeighbors" classifier was used in the Jupyter notebook.

3.5.8. Naive Bayes (NB)

The NB statistical classification method is based on the concept of conditional probability, where the attributes are assumed to be independent of each other (Soni et al., 2011). It allows the user to estimate the necessary parameters for classification with a minimal amount of training data (Bhargavi and Jyothi, 2009). To run the model, the "GaussianNB" classifier was used in the Jupyter notebook.

3.5.9. Light gradient boost machine (LightGBM)

LightGBM is a tree-based gradient-boosting framework. Exclusive feature bundling (EFB) and Gradient-based one-side sampling (GOSS), are two unique approaches used to make it distributed and efficient (Ke et al., 2017). LightGBM features are higher efficiency, quicker training speed, lower memory use, the capacity to handle large-scale data, better accuracy, and support for parallel and GPU learning compared to other methods (Rufo et al., 2021). To run the model, the "LGBM" classifier was used in the Jupyter notebook.

3.5.10. CatBoost classifier (CBC)

CBC is a relatively new gradient-boosting algorithm which uses binary decision trees as base predictors (Prokhorenkova et al., 2017). CBC identifies the gradient bias and prediction shift, which improves the algorithm's accuracy and generalization ability (Lu et al., 2022). To run the model, the "CatBoost" classifier was used in the Jupyter notebook.

3.6. Model validation and performance

One of the most important steps in developing a ML model is validating its performance (Garosi et al., 2019; Kariminejad et al., 2020). In this paper, validation of the model's accuracy is performed by analyzing the Area under the Curve (AUC) metrics associated with the Receiving Operating Characteristics (ROC) curves. The ROC curve is a diagnostic test usually adopted for the development of ML models (Golkarian et al., 2018) because it shows the true and false positive rates on the X-axis and Y-axis, respectively (Golkarian et al., 2018; Youssef et al., 2016). The value of the AUC ranges from 0 to 1, and the higher the value, the better the performance of the model (Chen et al., 2018; Golkarian et al., 2018; Youssef et al., 2016). If a model achieves a low positive prediction rate, it means that it cannot predict the actual data correctly. The contingency matrix and measures calculated for this study are shown in Table 3.

The Mean Square Error (MSE), Route Mean Square Error (RMSE), Mean Absolute Error (MAE), and coefficient of determination (R^2) were calculated to provide a comprehensive overview of the model's performance, enabling the identification of the best (lowest values of RMSE and MSE, and highest value of R^2) and worst (highest values of RMSE and MSE, and lowest value of R^2) models (Chicco et al., 2021). The detailed flowchart of this study is presented in Fig. 4.

Table 3
Detail description of the contingency matrix and different accuracy calculation.

		True class		
		Positive	Negative	Measures
Predictive Class	Positive	True Positive TP	False Positive FP	Positive Predictive Rate $\frac{TP}{TP+FP}$
	Negative	False Negative FN	True Negative TN	Negative Predictive Rate $\frac{TN}{FN+TN}$
	Measures	Sensitivity $\frac{TP}{TP+FN}$	Specificity $\frac{TN}{FP+TN}$	Accuracy $\frac{TP+TN}{TP+FP+FN+TN}$

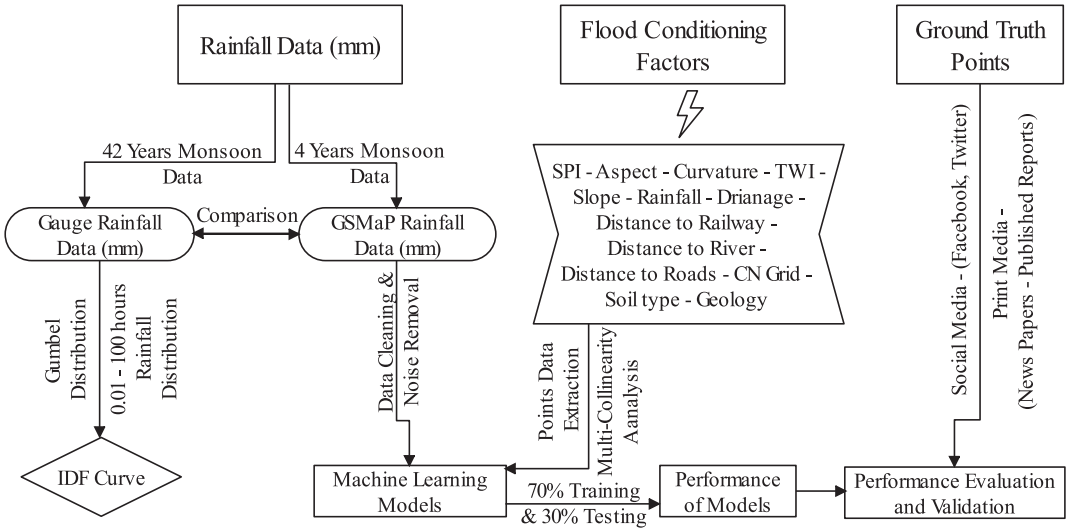

Fig. 4. Detailed flowchart of the present study.

4. Results

4.1. Comparison of stations gauged and GSMaP rainfall data

Table 4 shows a comparison of daily precipitation amounts recorded by ground monitoring stations with GSMaP precipitation data for the period from 2017 to 2020. Coefficients of determination (R-squared) were calculated to derive proportional relationships between the two data sets. In addition, Fig. 5 shows the daily comparisons between ground-measured stations and GSMaP precipitation data. The correlation coefficients between the satellite- and ground-based data ranged from 0.82 to 0.87, indicating a strong positive correlation (Yoshimoto and Amarnath, 2017). In addition, the R-squared values for the comparisons were also high, ranging from 0.71 to 0.74, indicating that the satellite data explained a significant amount of the variance in the ground-based data. Based on these results, it can be concluded that GSMaP data are a reliable source of precipitation data and can be used with confidence for flood mapping (Priyambodoho et al., 2021).

4.2. Generation of IDF curves

The IDF curve results presented here provide useful information on the relationship between precipitation intensity, duration, and the probability of occurrence of a given amount of precipitation. The data cover a range from 5 min to 24 h and a range of return periods from 2 years to 100 years. The Gumbel method was used to estimate intensity in mm during different return periods. The results show that for a given return period, the intensity decreases as the duration of the precipitation increases. This is due to the fact that the atmosphere is better able to absorb and dissipate precipitation over a longer period of time. These results have important implications for hydraulic engineering, flood mapping, and floodplain management. They can contribute to flood risk assessment and the development of flood warning systems, which are critical to protecting people and property from the potentially devastating effects of flooding. Overall, the IDF curve results provide valuable information for everyone involved in flood risk management, from engineers and planners to emergency planners and policy makers.

The IDF curves graphically represent the probability of precipitation events with similar characteristics in terms of intensity, duration, and return period, and serve as an effective representation of the maximum expected event in an area by reflecting the average rainfall intensity for different event durations at each return period (Mahdi and Mohamedmeki, 2020). The IDF curves offer a mathematical connection between the duration d, rainfall intensity i, and the return period T. This connection allows for the estimation of the return period of a particular observed rainfall event or, conversely, the rainfall intensity that corresponds to a given return period (Elsebaie, 2012).By considering the likely intensity and duration of rainfall events, they can make informed decisions about how best to protect communities from flood hazards.

Table 4
Comparison of daily stations gauged and GSMaP rainfall data.

Stations	Correlation coefficient	R-Square
Airport	0.87	0.74
PAF Base	0.85	0.73
Bin Qasim	0.82	0.71

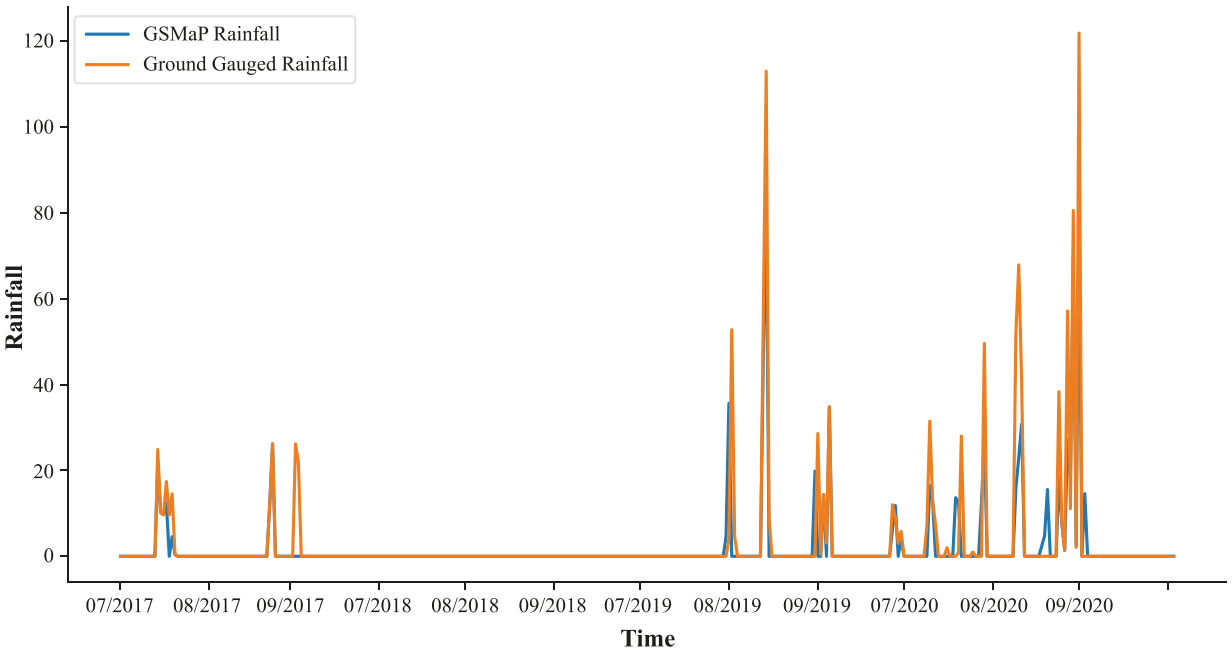

Fig. 5. Comparative graph of ground gauged and GSMap daily rainfall amount.

The IDF curve and distribution details for different return periods of Karachi Airport station is shown in Fig. 6 and Table 5. Upon analyzing the table, results shows that the rainfall intensity decreases as the duration of the rainfall event increases for a given return period. Similarly, an increase in the return period results in a higher rainfall intensity for a given duration. The highest rainfall intensity is recorded for shorter durations and higher return periods, while the lowest intensity is observed for longer durations and lower return periods. The intensity and duration of precipitation are shown on the y-axis and x-axis, respectively.

4.3. Feature selection and importance

Feature selection is a crucial step in machine learning applications due to the large number of variables in modern data sets that may not be relevant to the classification (Kursa and Rudnicki, 2010). Dealing with overlarge feature sets can lead to technical and accuracy issues, including algorithm slowdowns, resource consumption, and decreased accuracy when the number of variables is significantly higher than optimal (Kohavi and John, 1997). Analysis of flood conditioning factors using the ETC revealed that distance to the river, distance to the railway, aspect, and drainage, were the most important factors in predicting flood events. These factors had importance values of 0.106, 0.095, 0.093, and 0.092, respectively, indicating that these factors have a strong influence on the general occurrence and severity of flooding in the study area. Other factors such as SPI, distance to roads, TWI, curvature, and CNGrid were also found to be important, but to a lesser extent. These factors had importance values ranging from 0.058 to 0.092, indicating that

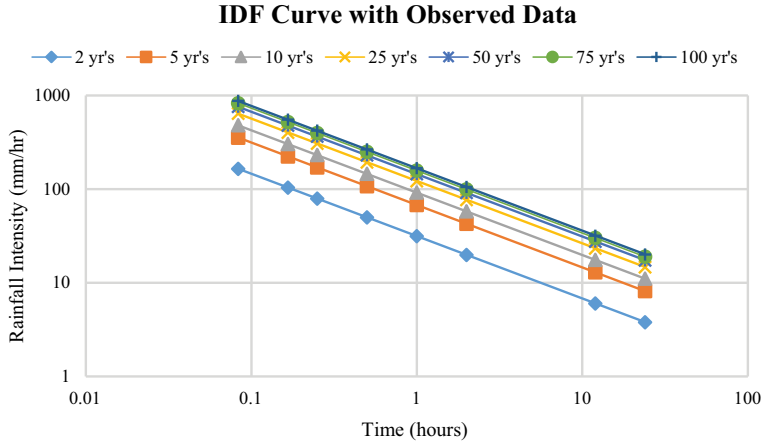

Fig. 6. IDF curve with Gumbel distribution technique for observed data.

Table 5
The rainfall intensity of different years returns periods using Gumbel distribution.

Duration (min)	Rainfall intensity (mm/h)						
	Return periods (Years)						
	2	5	10	25	50	75	100
5	164.92	355.21	481.20	640.39	758.49	827.13	875.71
10	103.89	223.77	303.14	403.42	477.82	521.06	551.66
15	79.28	170.77	231.34	307.87	364.64	397.64	421.00
30	49.95	107.58	145.73	193.94	229.71	250.50	265.21
60	31.46	67.77	91.81	122.18	144.71	157.80	167.07
120	19.82	42.69	57.83	76.97	91.16	99.41	105.25
720	6.00	12.93	17.52	23.31	27.61	30.11	31.88
1440	3.78	8.14	11.03	14.68	17.39	18.97	20.08

they may also play a role in predicting flood events, but their influence is likely less pronounced than that of the most important factors. Finally, soil, geology, and slope were identified as the least important factors in predicting flood events, with importance values of 0.053, 0.052, and 0.054, respectively.

These factors may still contribute to our understanding of flood events, but their influence is likely minimal compared to other factors. The importance ranking of these factors has been used as the basis for various forecasting techniques and can be used to improve flood risk management and mitigation strategies by providing insight into the key factors that contribute to flood vulnerability in the study area. These factors can also be used to develop more accurate and robust flood prediction models that can be useful for disaster management and emergency response. Fig. 7 describes the factors that were found to be important and selected for the models from ML.

4.4. Model's performance

In this study, ten different ML models were used to predict the UPF inundation points, using two measures of performance, training accuracy and validation accuracy. The models used were LightGBM, RF, NN's, LG, XGBoost, SVM, KNN, CBC, NB, and DT. Training accuracy measures how well a model fits the data on which it was trained, while validation accuracy measures how well a model generalizes to new, unseen data. The performance of each model was evaluated using ROC and AUC curves, where AUC is a measure of how well the model can discriminate between positive and negative examples. Higher AUC values indicate better performance.

The results of the study showed that LightGBM had the highest AUC value for the training models with an AUC value of 0.907. RF and NNs followed closely behind with AUC values of 0.904 and 0.899, respectively. LG, XGBoost, SVM, KNN, CBC, NB, and DT had lower AUC values, with DT having the lowest AUC value of 0.817. To assess the predictive performance of each model, the validation accuracy was also evaluated separately. Among the validation models, CBC had the highest AUC value with an AUC value of 0.855. LG was followed by SVM, DT, and NN with AUC values of 0.850, 0.848, 0.847, and 0.841, respectively. RF, lightGBM, XGBoost, NB, and KNN had lower AUC values, with KNN having the lowest AUC value of 0.746.

The overall ranking of the models based on their validation accuracy was CBC, LG, SVM, DT, NNs, RF, lightGBM, XGBoost, NB, and KNN. The study also shows the importance of carefully selecting the ML model used for the task, as different models may perform better or worse depending on the dataset and the task. Fig. 8 shows the performance of each model, with the black line representing the

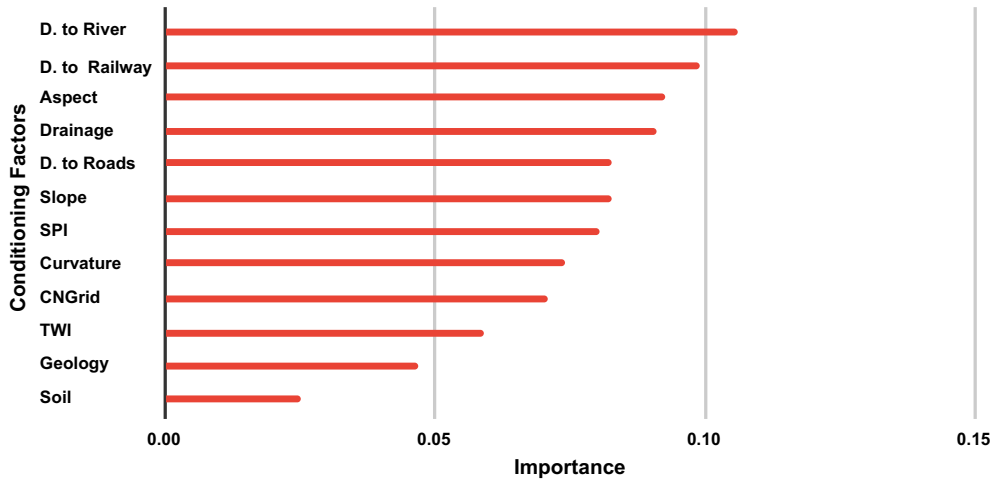

Fig. 7. Selected conditioning factors in ETC and their importance.

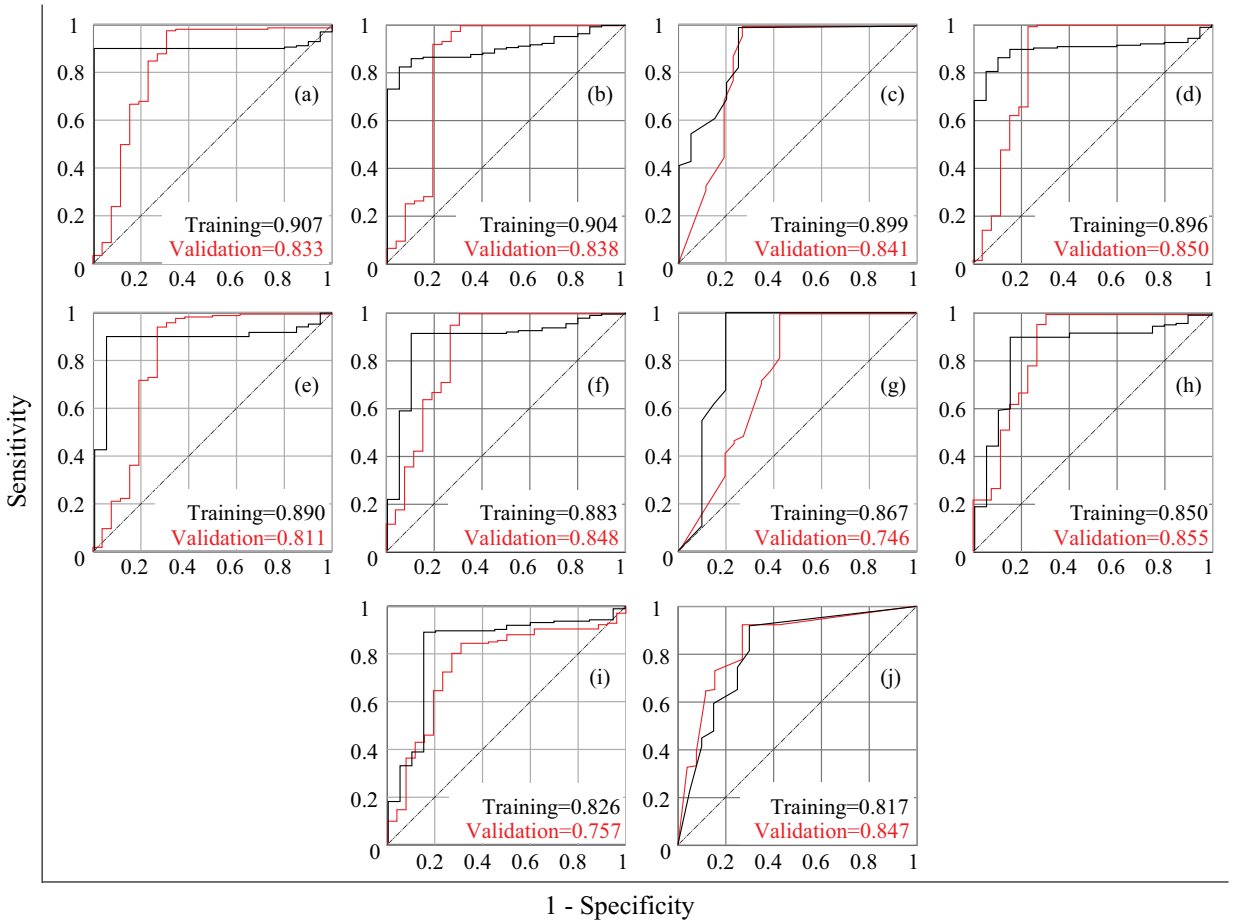

Fig. 8. Accuracy of the training models and accuracy of validation models of the selected models (see Table 2) (a) LightGBM, (b) RF, (c) NN's, (d) LG, (e) XGBoost, (f) SVM, (g) KNN, (h) CBC, (i) NB and (j) DT.

ROC curve of the training dataset and the red line representing the ROC curve of the validation dataset. The AUC values were used to determine the accuracy of each model for both the training and validation datasets.

Table 6 shows the results of a comparison between ten different ML models based on a different evaluation where the top values represent the training values, while the bottom values represent the validations values. The models compared are LightGBM, RF, NN's, LG, XGBoost, SVM, KNN, CBC, NB, and DT.

When analyzing the RMSE, the best models are CBC, NN's, and LG with RMSE values of 0.276/0.233, 0.282/0.267, and 0.298/0.233, respectively. The models with the worst RMSE values are NB and DT, with RMSE values of 0.319/0.389 and 0.368/0.328. In MAE, the best models are KNN, RF, and NN with MAE values of 0.068/0.119, 0.114/0.152, and 0.125/0.072, respectively. The models

Table 6
Detailed summary of TPR, TNR, PPR, NPR, MSE, RMSE, MAE, and R^2 of the training and validation models.

Models	RMSE	MAE	MSE	R2	TPR	TNR	PPR	NPR	ACC
	T/V	T/V	T/V	T/V	T/V	T/V	T/V	T/V	T/V
LightGBM	0.302/0.267	0.179/0.126	0.086/0.071	1/0.838	0.977/0.982	0.888/0.809	0.988/0.976	0.8/0.85	0.968/0.963
RF	0.293/0.239	0.114/0.152	0.048/0.057	1/0.875	0.976/0.988	0.842/0.782	0.982/0.97	0.8/0.9	0.963/0.963
NN's	0.282/0.267	0.125/0.072	0.091/0.071	0.841/0.89	0.964/0.976	0.56/0.727	0.936/0.965	0.7/0.8	0.911/0.947
LG	0.298/0.233	0.188/0.145	0.076/0.05	0.901/0.869	0.965/0.976	0.736/0.761	0.97/0.97	0.7/0.8	0.942/0.953
XGBoost	0.303/0.262	0.186/0.126	0.102/0.068	1/0.828	0.988/0.988	0.947/0.9	0.994/0.988	0.9/0.9	0.984/0.979
SVM	0.285/0.235	0.126/0.16	0.087/0.055	0.895/0.875	0.982/0.971	0.708/0.789	0.959/0.976	0.85/0.75	0.947/0.953
KNN	0.291/0.259	0.068/0.119	0.066/0.067	0.901/0.869	0.976/0.97	0.727/0.714	0.965/0.965	0.8/0.75	0.947/0.942
CBC	0.276/0.233	0.141/0.126	0.076/0.054	0.994/0.875	0.988/0.982	0.857/0.809	0.982/0.976	0.9/0.85	0.973/0.963
NB	0.319/0.389	0.123/0.229	0.106/0.151	0.838/0.76	0.946/0.949	0.458/0.363	0.924/0.877	0.55/0.6	0.885/0.848
DT	0.368/0.328	0.196/0.129	0.088/0.107	0.979/0.802	0.965/0.958	0.7/0.565	0.965/0.941	0.7/0.65	0.937/0.911

T: Training; V: Validation.

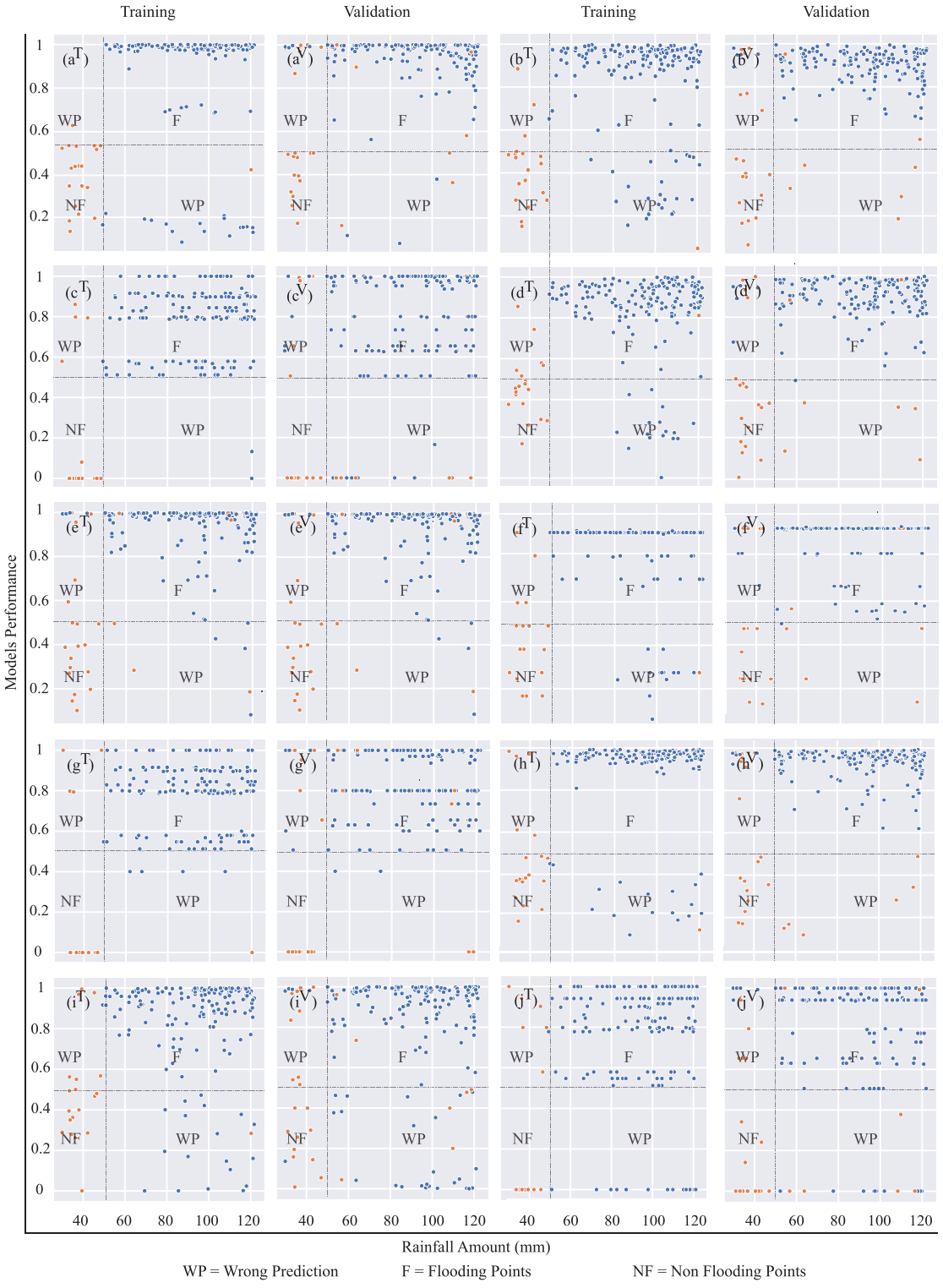

Fig. 9. Performance of all ML models during the training and validation (a) LightGBM, (b) RF, (c) NN's, (d) LG, (e) XGBoost, (f) SVM, (g) KNN, (h) CBC, (i) NB and (j) DT.

with the lowest performance in terms of MAE are LG and NB, with MAE values of 0.188/0.145 and 0.123/0.229, respectively. The models with the best MSE values are RF and KNN, with MSE values of 0.048/0.057 and 0.066/0.067, respectively. The model with the worst MSE value is NB, with a value of 0.106/0.151. The R^2 measures the proportion of variance in the dependent variable that is predictable by the independent variable(s). The model with the highest R^2 value is CBC, with a value of 0.994/0.875, while the model with the lowest R^2 value is NN's, with a value of 0.841/0.89.

The metrics TPR and TNR matrix measure the ability of the models to correctly identify positive and negative cases, respectively. The best-performing models in terms of TPR are XGBoost and CBC with TPR values of 0.988/0.988 and 0.988/0.982, respectively. The models with the best TNR performance are LG and RF, with TNR values of 0.736/0.761 and 0.842/0.782, respectively. The metrics PPR and NPR matrix measure the proportion of true positives and true negatives among all predicted positives and negatives, respectively. The model with the highest PPR score is XGBoost, with a score of 0.994/0.988, while the model with the lowest PPR score is NB, with a score of 0.924/0.877. The model with the highest NPR score is SVM, with a score of 0.85/0.75, while the model with the lowest NPR score is NB, with a score of 0.55/0.6.

Finally, the metric ACC measures the overall accuracy of the models in predicting the target variable. The model with the highest accuracy score is XGBoost, with a score of 0.984/0.979, while the model with the lowest accuracy score is NB, with a score of 0.885/0.848.

4.5. Comparative performance of ML models

The results of the study showed that ML models can effectively predict the inundated area of UPF, with some models performing better than others. Fig. 9 shows the correlation between rainfall amount and the performance of ten different ML models in predicting flooding and non-flooding points. The graph shows that as the amount of rainfall increases, the performance of the models also increases. This type of correlation between prediction and actual values indicates model performance and helps evaluate ML techniques.

Fig. 9 also describes the performance of the models at the training and validation levels, with blue and orange colors representing flooding and non-flooding events, respectively. The x-axis shows the amount of precipitation with values ranging from 0 to 145 mm. The y-axis represents model performance, with values ranging from 0 to 1. The x-axis represents the amount of precipitation, with values above 50 mm indicating a flooding event and values below 50 mm indicating a non-flooding event. The y-axis represents the performance of the models as measured by the proportion of correctly predicted events. The range of correct prediction was set to 0.5, meaning that any prediction that falls within the range of 0.5 is considered correct.

The models with the best accuracy are CBC, XGBoost, and NN with accuracy between 0.8 and 0.95 for precipitation amounts above 50 mm. However, for precipitation amounts below 50 mm, the performance of the models decreases significantly, with accuracy ranging from 0.2 to 0.7. Overall, the graph suggests that while the models perform well in predicting high rainfall flood events, they struggle in predicting low rainfall non-flood events. This information could be useful for developing targeted flood forecasting systems that focus on areas with high rainfall and for improving the accuracy of flood forecasting models in areas with low rainfall. It is important to note that ML models are data-based methods that are highly dependent on the quantity and quality of available data. Therefore, it is important to carefully select and evaluate the performance of the various ML models for each specific context.

5. Discussion

Flooding is an unpredictable, naturally occurring phenomenon that significantly impacts life and socioeconomic growth in vulnerable areas. However, a lack of understanding of the spatial volatility of floods can lead to inadequate flood management. The Islamic Republic of Pakistan is a highly vulnerable country to natural disasters, especially floods. Pakistan has experienced approximately 38 floods of varying magnitude (including 19 severe floods). Increased flooding poses a serious problem to the economic sustainability and long-term growth of cities due to its impact on residential, industrial, agricultural, and other infrastructure needs (Bazai and Panezai, 2020). The study area has experienced significant flood events since the mid-1980s and especially in the last decade.

Flood mapping, is particularly critical to flood risk management and mitigation. Numerous factors affect the occurrence of pluvial flooding, such as rainfall, natural and urban drainage system, growth of urbanized areas, capacity of water retention in drains, etc. However, there is no evidence that pluvial flooding is only due to changing precipitation patterns. According to Spekkers et al. (2013), precipitation alone cannot explain the intensity of floods. Therefore, various phenomena and factors are critical to understanding the magnitude of flooding. This research contributes to a better understanding of these factors by using ML models to evaluate the effects of factors affecting flooding in modeling and to identify the contribution of variables (Torrence and Compo, 1998). Due to the complex nature of data in flood modeling, it can be challenging to select the most effective and powerful ML algorithm (Mohammadi et al., 2018).

The results of this study suggest that certain environmental and topographical factors play an important role in predicting flood events. The study found that distance to the river (Chen et al., 2019a), distance to the railway, aspect, and drainage (Paul et al., 2019) were the most important factors in predicting flood events, with values ranging from 0.106 to 0.092. These results are consistent with previous studies (Shafizadeh-Moghadam et al., 2018) that identified proximity to water bodies and elevation as important predictors of flooding and Collins et al. (2022) suggesting that these are the factors thought to be responsible for flood damage in different geographic regions. Previous studies have also identified land use and topography as important predictors of flooding (Dalu et al., 2018). The least important factors in predicting flood events were soil, geology, and slope, with significance values ranging from 0.054 to 0.052 but these factors can also contribute during the flood, such as slope in the flat areas and due to their low flow resistance,

coastal regions are prone to flooding (Lei et al., 2021). Despite minimal influence from geology, the other factors affecting flooding include drainage density, rainfall, LC, slope, and NDVI, as confirmed by previous studies (Chowdhuri et al., 2020; Roy et al., 2020). These factors may still contribute to our understanding of flood events, but their influence is likely minimal compared to other factors.

According to the different statistical evaluation criteria used in this study, LightGBM (0.907), RF (0.904) and NN's (0.899) in the training models and CBC (0.855), LG (850) and SVM (0.848) in the prediction models showed the higher accuracy compared to other models, which is consistent with previous studies (Abedi et al., 2022; Rasool et al., 2020). Mirzaei et al. (2021b) and Naghibi et al. (2020) conducted studies in Iran and found that Gradient Boost and RF were the most effective models with a predictive accuracy of 98% and 97.1%, respectively. Naghibi et al. (2020) emphasized that the KNN model had higher accuracy with an AUC of 94.6%. These results are consistent with our results, in which the KNN model had an AUC of 86.7%.

According to previous studies, the lower the values of RMSE, MSE, and MAE, the better the performance of the predictive models (Pedregosa et al., 2011). In the present study, most of the models from ML had lower model prediction error, such as CBC, NN, and LG with RMSE values of 0.233, 0.267, and 0.233; KNN, RF, and NN with MAE values of 0.119, 0.152, and 0.072, respectively; and RF and KNN with MSE values of 0.057 and 0.067, respectively. Higher R2 values also indicate that the selected models perform well in training and prediction. The model with the highest R2 value is CBC with a value of 0.875, while the model with the lowest R2 value is that of NN, with a value of 0.89 (Rokach, 2010).

Fig. 10 shows the performance of prediction points and flooded locations in specific years. However, the limited number of records of flood events has affected the performance of the TPR as well as the various models used in data processing and handling. This is because misclassifications of flooded and non-flooded points can occur. For example, flooding caused by blockage of drainage systems along roads and streets may be misidentified as flooding due to rainfall, leading to an increase in the number of false positives (Ten Veldhuis et al., 2013). Eliminating false flood reports is not an easy task because recent rainfall reports do not provide information on the causes of flooding. Therefore, data must be better managed to minimize errors in identifying floodplains. One of the possible strategies to minimize the number of false positive reports is to supplement the existing flood data with other data sources, such as social media data and other information provided by a variety of people. Models can be improved at the district, community, or street level as more data become available.

Integrating complex interactions between the natural and built environments into machine and deep learning models is a challenging task (Bentivoglio et al., 2022).While advanced technologies have supported the development of flood models, there are still uncertainties and limitations in the spatial analysis methods used in such models (Yan et al., 2023). The original data are prone to errors, while the estimated data are subject to uncertainties and therefore limited in their use in modeling (Teng et al., 2017). For example, fine urban meteorological data and surface parameters such as depression storage, Manning roughness coefficient, and soil texture are usually obtained from local ground stations and sampling sites. Insufficient sample density and imperfect upscaling methods often lead to uncertainties in extrapolating such data to a large area (Zhang, 2007).

When multiple data of different types and origins are input into a flood model, converting the data into uniform formats, such as numerical format and the same resolution and geographic projection, inevitably leads to discrepancies (Meliho et al., 2021). In addition, the availability of certain technologies and approaches that can potentially provide inundation area and inundation depth information does not cover all areas and cases, making flood model validation and uncertainty assessment challenging, especially for small floodplains (Yan et al., 2023).

6. Conclusion and recommendations

This study provides valuable insights into UPF risk management in the Karachi region of Pakistan. The IDF curves using the Gumbel method provided a better understanding of the relationship between rainfall intensity, duration, and the probability of occurrence of a given amount of rainfall. The study highlights the importance of the careful selection of influencing factors for flood events and found that distance to the river, distance to the railway, aspect, and drainage as the most important factors. Ten ML models were evaluated in predicting urban flood inundation points varied based on the dataset and task, emphasizing the significance of meticulous model selection, evaluated through training accuracy and validation accuracy. The model training and validation process involved 384 pluvial flooding inundation points. The LightGBM, RF, and NNs were found to have the highest AUC scores for the training models and scoring 0.907, 0.904 and 0.899, respectively while CBC had the highest AUC score at 0.855 for the validation models. The overall ranking of the models based on their validation accuracy was CBC, LG, SVM, DT, NNs, RF, LightGBM, XGBoost, NB, and KNN. The models with the lowest RMSE values were CBC, NNs, and LG, highlighting their potential for developing accurate and robust models for predicting flood events.

It is determined that ML models can quantify the rainfall amount as a line projected that is divided into two principal components, obtaining a binary result (flood or no flood). The study's findings suggest that the accuracy of the models is dependent on the amount and quality of available data, as well as the specific context of the area being studied. The results of this study have important implications for disaster management and emergency response in the Karachi region, particularly for pluvial flood risk assessment and flood warning system development. This study's findings could be used to improve flood risk management strategies by providing more accurate predictions of potential flood events, enabling authorities to take appropriate preventative measures in advance. By incorporating the likely intensity and duration of rainfall events, as well as carefully selected influencing factors, into flood event prediction models, decision-makers can make informed decisions about how best to protect communities from flood hazards. Finally, the study's emphasis on the importance of data quality and quantity can encourage researchers to gather more comprehensive and high-quality data to improve the accuracy of urban flood prediction models.

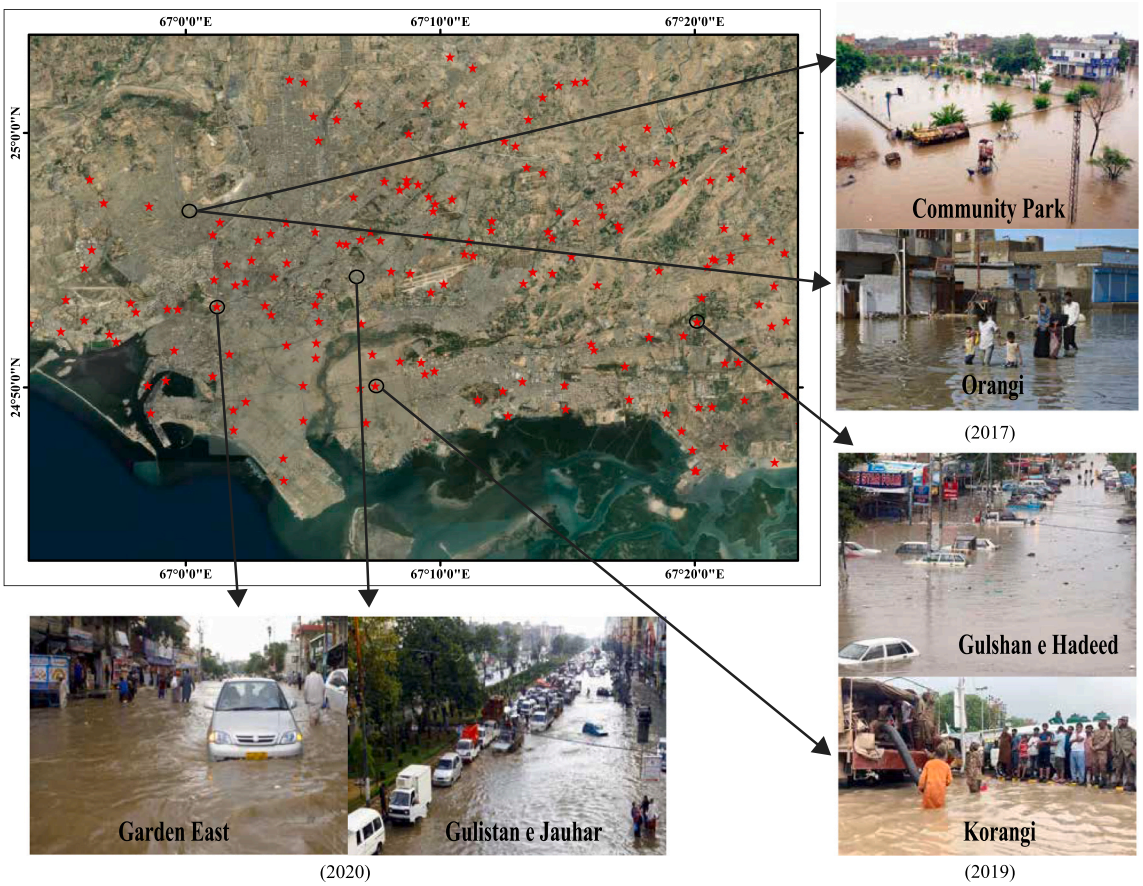

Fig. 10. Performance of ML models prediction along with multiple flooded locations in the study area.

Author contribution

Umair Rasool: Conceptualization, Data curation, Writing – original draft, Investigation, Methodology, Software, Validation; Xinan Yin: Writing - Review & editing, Supervision; Zongxue Xu: Writing - Review & editing, Supervision, Funding acquisition; Roberta Padulano: Writing - Review & editing; Muhammad Awais Rasool: Conceptualization, Writing - Review & editing; Muhammad Amir Siddique: Formal analysis; Muhammad Azher Hassan: Software, Formal analysis; Venkatramanan Senapathi: Writing - Review & editing.

Declaration of Competing Interest

The authors declare that they have no known competing financial interests or personal relationships that could have appeared to influence the work reported in this paper.

Data availability

Data will be made available on request.

Acknowledgments

The authors are thankful to the Pakistan Meteorological Department (PMD) to provided precipitation data and Survey of Pakistan for providing us with different types of vector data for the present study, and the United States Geological Survey (USGS) for providing the free DEM and Sentinel-2 images via google earth engine. The authors are also thankful to the National Natural Science Foundation of China (52239003) for providing the funding for this research.

References

Abedi, R., Costache, R., Shafizadeh-Moghadam, H., Pham, Q.B., 2022. Flash-flood susceptibility mapping based on XGBoost, random forest and boosted regression trees. Geocarto Int. 37 (19), 5479–5496.

Abeshu, G.W., Li, H.-Y., Zhu, Z., Tan, Z., Leung, L.R., 2022. Median bed-material sediment particle size across rivers in the contiguous US. Earth Syst. Sci. Data 14 (2), 929–942.

Abood, H.G., Salman, G.A., 2021. Utilizing variance inflation factor for electricity demand forecasting. In: Paper Presented at the Proceedings of Symposium on Power Electronic and Renewable Energy Systems Control: PERESC 2020.

Agonafir, C., 2022. A Citizen-Science Approach for Urban Flood Risk Analysis Using Data Science and Machine Learning. The City College of New York.

Ahammed, F., Hewa, G.A., Argue, J.R., 2014. Variability of annual daily maximum rainfall of Dhaka, Bangladesh. Atmos. Res. 137, 176–182.

Ahmad, M., Al Mehedi, M.A., Yazdan, M.M.S., Kumar, R., 2022. Development of machine learning flood model using artificial neural network (ANN) at Var River. Liquids 2 (3), 147–160.

Ahmed, Q.I., Lu, H., Ye, S., 2008. Urban transportation and equity: a case study of Beijing and Karachi. Transp. Res. A Policy Pract. 42 (1), 125–139.

Asadollah, S.B.H.S., Sharafati, A., Motta, D., Yaseen, Z.M., 2021. River water quality index prediction and uncertainty analysis: a comparative study of machine learning models. J. Environ. Chem. Eng. 9 (1), 104599.

Azizi, K., Diko, S.K., Saija, L., Zamani, M.G., Meier, C.I., 2022. Integrated community-based approaches to urban pluvial flooding research, trends and future directions: a review. Urban Clim. 44, 101237.

Bakhsh, H.A., Shakir, A.S., Khan, N.M., 2011 Jul. Flood inundation modeling for Malir watershed of Karachi considering future mean sea level rise. Pak. J. Eng. Appl. Sci. 9, 34–47.

Bank, W, 2018. Transforming Karachi into a Livable and Competitive Megacity: A City Diagnostic and Transformation Strategy. The World Bank.

Bazai, M.H., Panezai, S., 2020. Assessment of urban sprawl and land use change dynamics through GIS and remote sensing in Quetta, Balochistan, Pakistan. J. Geogr. Soc. Sci. 2 (1), 20.

Benhammou, Y., Alcaraz-Segura, D., Guirado, E., Khaldi, R., Achchab, B., Herrera, F., Tabik, S., 2022. Sentinel2GlobalLULC: a Sentinel-2 RGB image tile dataset for global land use/cover mapping with deep learning. Sci. Data 9 (1), 681.

Bentivoglio, R., Isufi, E., Jonkman, S.N., Taormina, R., 2022. Deep learning methods for flood mapping: a review of existing applications and future research directions. Hydrol. Earth Syst. Sci. 26 (16), 4345–4378.

Bhargavi, P., Jyothi, S., 2009. Applying naive bayes data mining technique for classification of agricultural land soils. Int. J. Comput. Sci. Netw. Secur. 9 (8), 117–122.

Bhatti, M.W., 2021. Heavy Showers Cause Flooded Roads, Traffic Jams in Karachi. Retrieved from. https://www.thenews.com.pk/print/894874-heavy-showers-cause-flooded-roads-traffic-jams-in-karachi.

Bouramtane, T., Kacimi, I., Bouramtane, K., Aziz, M., Abraham, S., Omari, K., El Beqqali, O., 2021. Multivariate analysis and machine learning approach for mapping the variability and vulnerability of urban flooding: the case of Tangier City, Morocco. Hydrology 8 (4), 182.

Breiman, L., Friedman, J., Olshen, R., 2017. Classification and Regression Trees Routledge. Chapman and Hall CRC.

Brillinger, M., Dehnhardt, A., Schwarze, R., Albert, C., 2020. Exploring the uptake of nature-based measures in flood risk management: evidence from German federal states. Environ. Sci. Pol. 110, 14–23.

Bruwier, M., Maravat, C., Mustafa, A., Teller, J., Pirotton, M., Erpicum, S., Dewals, B., 2020. Influence of urban forms on surface flow in urban pluvial flooding. J. Hydrol. 582, 124493.

Ceballos, F., 2019. An Intuitive Explanation of Random Forest and Extra Trees Classifiers. Medium. July, 17.

Chen, W., Li, H., Hou, E., Wang, S., Wang, G., Panahi, M., Niu, C., 2018. GIS-based groundwater potential analysis using novel ensemble weights-of-evidence with logistic regression and functional tree models. Sci. Total Environ. 634, 853–867.

Chen, W., Panahi, M., Tsangaratos, P., Shahabi, H., Ilia, I., Panahi, S., Ahmad, B.B., 2019a. Applying population-based evolutionary algorithms and a neuro-fuzzy system for modeling landslide susceptibility. Catena 172, 212–231.

Chen, H., Yong, B., Gourley, J.J., Liu, J., Ren, L., Wang, W., Zhang, J., 2019b. Impact of the crucial geographic and climatic factors on the input source errors of GPM-based global satellite precipitation estimates. J. Hydrol. 575, 1–16.

Cheng, D., Zhang, S., Deng, Z., Zhu, Y., Zong, M., 2014. kNN algorithm with data-driven k value. In: Paper presented at the International Conference on Advanced Data Mining and Applications.

Chicco, D., Warrens, M.J., Jurman, G., 2021. The coefficient of determination R-squared is more informative than SMAPE, MAE, MAPE, MSE and RMSE in regression analysis evaluation. PeerJ Comput. Sci. 7, e623.

Choubin, B., Moradi, E., Golshan, M., Adamowski, J., Sajedi-Hosseini, F., Mosavi, A., 2019. An ensemble prediction of flood susceptibility using multivariate discriminant analysis, classification and regression trees, and support vector machines. Sci. Total Environ. 651, 2087–2096.

Chowdhuri, I., Pal, S.C., Chakrabortty, R., 2020. Flood susceptibility mapping by ensemble evidential belief function and binomial logistic regression model on river basin of eastern India. Adv. Space Res. 65 (5), 1466–1489.

City District Government Karachi, C, 2007. Karachi Strategic Development Plan 2020. CDGK Karachi.

Collins, E.L., Sanchez, G.M., Terando, A., Stillwell, C.C., Mitasova, H., Sebastian, A., Meentemeyer, R.K., 2022. Predicting flood damage probability across the conterminous United States. Environ. Res. Lett. 17 (3), 034006.

Costache, R., Arabameri, A., Elkhrachy, I., Ghorbanzadeh, O., Pham, Q.B., 2021. Detection of areas prone to flood risk using state-of-the-art machine learning models. Geomat. Nat. Hazards Risk 12 (1), 1488–1507.

Cover, T., Hart, P., 1967. Nearest neighbor pattern classification. IEEE Trans. Inf. Theory 13 (1), 21–27.

Dalu, M.T., Shackleton, C.M., Dalu, T., 2018. Influence of land cover, proximity to streams and household topographical location on flooding impact in informal settlements in the eastern cape, South Africa. Int. J. Disaster Risk Reduct. 28, 481–490.

Darabi, H., Choubin, B., Rahmati, O., Haghighi, A.T., Pradhan, B., Kløve, B., 2019. Urban flood risk mapping using the GARP and QUEST models: a comparative study of machine learning techniques. J. Hydrol. 569, 142–154.

Das, J., Mandal, T., Rahman, A.S., Saha, P., 2021. Spatio-temporal characterization of rainfall in Bangladesh: an innovative trend and discrete wavelet transformation approaches. Theor. Appl. Climatol. 143 (3–4), 1557–1579.

Drover, D., Howcroft, J., Kofman, J., Lemaire, E.D., 2017. Faller classification in older adults using wearable sensors based on turn and straight-walking accelerometer-based features. Sensors 17 (6), 1321.

Elsebaie, I.H., 2012. Developing rainfall intensity–duration–frequency relationship for two regions in Saudi Arabia. J. King Saud Univ. Eng. Sci. 24 (2), 131–140.

Fernández, D., Lutz, M.A., 2010. Urban flood hazard zoning in Tucumán Province, Argentina, using GIS and multicriteria decision analysis. Eng. Geol. 111 (1–4), 90–98.

Garosi, Y., Sheklabadi, M., Conoscenti, C., Pourghasemi, H.R., Van Oost, K., 2019. Assessing the performance of GIS-based machine learning models with different accuracy measures for determining susceptibility to gully erosion. Sci. Total Environ. 664, 1117–1132.

Gayen, A., Pourghasemi, H.R., Saha, S., Keesstra, S., Bai, S., 2019. Gully erosion susceptibility assessment and management of hazard-prone areas in India using different machine learning algorithms. Sci. Total Environ. 668, 124–138.

Golkarian, A., Naghibi, S.A., Kalantar, B., Pradhan, B., 2018. Groundwater potential mapping using C5. 0, random forest, and multivariate adaptive regression spline models in GIS. Environ. Monit. Assess. 190 (3), 1–16.

Goodfellow, I., Bengio, Y., Courville, A., 2016. Deep Learning. MIT Press.

Hall, M.A., Smith, L.A., 1999. Feature selection for machine learning: comparing a correlation-based filter approach to the wrapper. In: Paper Presented at the FLAIRS Conference.

HANDS, 2020. Rapid Need Assessment Urban Flooding Karachi - July 2020. Retrieved from. https://reliefweb.int/report/pakistan/rapid-need-assessment-urban-flooding-karachi-july-2020.

Haq, U., 2014. The Rise of Karachi as a Mega-City: Issues and Challenges. Human development centre. Retrieved from. http://www.mhhdc.org.
Hasan, A., Ahmed, N., Raza, M., Sadiq, A., Ahmed, S., Sarwar, M.B., 2013. Land Ownership, Control and Contestation in Karachi and Implications for Low-Income Housing. International Institute for Environment and Development London.
Hawkins, R.H., Theurer, F.D., Rezaeianzadeh, M., 2019. Understanding the basis of the curve number method for watershed models and TMDLs. J. Hydrol. Eng. 24 (7), 06019003.
Huang, H., Zhuo, L., Li, Z., Ji, X., Wu, P., 2023. Effects of multidimensional urbanisation on water footprint self-sufficiency of staple crops in China. J. Hydrol. 618, 129275.
Hutchinson, R., Liu, L.-P., Dietterich, T., 2011. Incorporating boosted regression trees into ecological latent variable models. In: Paper Presented at the Proceedings of the AAAI Conference on Artificial Intelligence.
Islam, A.R.M.T., Talukdar, S., Mahato, S., Kundu, S., Eibek, K.U., Pham, Q.B., Linh, N.T.T., 2021. Flood susceptibility modelling using advanced ensemble machine learning models. Geosci. Front. 12 (3), 101075.
Kareem, D.A., Amen, A.R.M., Mustafa, A., Yüce, M.I., Szydłowski, M., 2022. Comparative analysis of developed rainfall intensity–duration–frequency curves for Erbil with other Iraqi urban areas. Water 14 (3), 419.
Kariminejad, N., Hosseinalizadeh, M., Pourghasemi, H.R., Ownegh, M., Rossi, M., Tiefenbacher, J.P., 2020. Optimizing collapsed pipes mapping: effects of DEM spatial resolution. Catena 187, 104344.
Ke, G., Meng, Q., Finley, T., Wang, T., Chen, W., Ma, W., Liu, T.-Y., 2017. Lightgbm: A highly efficient gradient boosting decision tree. Adv. Neural Inf. Proces. Syst. 30, 3146–3154.
Ke, Q., Tian, X., Bricker, J., Tian, Z., Guan, G., Cai, H., Liu, J., 2020. Urban pluvial flooding prediction by machine learning approaches–a case study of Shenzhen city, China. Adv. Water Resour. 145, 103719.
Kim, J.-C., Jung, H.-S., Lee, S., 2018. Groundwater productivity potential mapping using frequency ratio and evidential belief function and artificial neural network models: focus on topographic factors. J. Hydroinf. 20 (6), 1436–1451.
Kohavi, R., John, G.H., 1997. Wrappers for feature subset selection. Artif. Intell. 97 (1–2), 273–324.
Kron, W., Eichner, J., Kundzewicz, Z.W., 2019. Reduction of flood risk in Europe–reflections from a reinsurance perspective. J. Hydrol. 576, 197–209.
Kursa, M.B., Rudnicki, W.R., 2010. Feature selection with the Boruta package. J. Stat. Softw. 36, 1–13.
Lei, X., Chen, W., Panahi, M., Falah, F., Rahmati, O., Uuemaa, E., Tiefenbacher, J.P., 2021. Urban flood modeling using deep-learning approaches in Seoul, South Korea. J. Hydrol. 601, 126684.
Ling, L., Yusop, Z., Chow, M.F., 2020. Urban flood depth estimate with a new calibrated curve number runoff prediction model. IEEE Access 8, 10915–10923.
Lu, C., Zhang, S., Xue, D., Xiao, F., Liu, C., 2022. Improved estimation of coalbed methane content using the revised estimate of depth and CatBoost algorithm: a case study from southern Sichuan Basin, China. Comput. Geosci. 158, 104973.
Mahdi, E.S., Mohamedmeki, M.Z., 2020. Analysis of rainfall intensity-duration-frequency (IDF) curves of Baghdad city. In: Paper Presented at the IOP Conference Series: Materials Science and Engineering.
Marelle, L., Myhre, G., Steensen, B.M., Hodnebrog, Ø., Alterskjær, K., Sillmann, J., 2020. Urbanization in megacities increases the frequency of extreme precipitation events far more than their intensity. Environ. Res. Lett. 15 (12), 124072.
Mega, T., Ushio, T., Takahiro, M., Kubota, T., Kachi, M., Oki, R., 2018. Gauge-adjusted global satellite mapping of precipitation. IEEE Trans. Geosci. Remote Sens. 57 (4), 1928–1935.
Mehedi, M.A.A., Smith, V., Hosseiny, H., Jiao, X., 2022. Unraveling the complexities of urban fluvial flood hydraulics through AI. Sci. Rep. 12 (1), 18738.
Mehravar, S., Razavi-Termeh, S.V., Moghimi, A., Ranjgar, B., Foroughnia, F., Amani, M., 2023. Flood susceptibility mapping using multi-temporal SAR imagery and novel integration of nature-inspired algorithms into support vector regression. J. Hydrol. 129100.
Meliho, M., Khattabi, A., Asinyo, J., 2021. Spatial modeling of flood susceptibility using machine learning algorithms. Arab. J. Geosci. 14, 18. https://doi.org/10.1007/s12517-021-08610-1.
Micheletti, N., Foresti, L., Kanevski, M., Pedrazzini, A., Jaboyedoff, M., 2011. Landslide susceptibility mapping using adaptive support vector machines and feature selection. In: Master Thesis Submitted to University of Lausanne Faculty of Geosciences and Environment for the Degree of Master of Science in Environmental Geosciences, p. 99.
Mirza, M.M.Q., 2003. Climate change and extreme weather events: can developing countries adapt? Clim. Pol. 3 (3), 233–248.
Mirzaei, S., Vafakhah, M., Pradhan, B., Alavi, S.J., 2021a. Flood susceptibility assessment using extreme gradient boosting (EGB), Iran. Earth Sci. Inf. 14 (1), 51–67.
Mirzaei, S., Vafakhah, M., Pradhan, B., Alavi, S.J., 2021b. Flood susceptibility assessment using extreme gradient boosting (EGB), Iran. Earth Sci. Inf. 14, 51–67.
Mohammadi, A., Shahabi, H., Bin Ahmad, B., 2018. Integration of insartechnique, google earth images and extensive field survey for landslide inventory in a part of Cameron highlands, Pahang, Malaysia. Appl. Ecol. Environ. Res. 16, 8075–8091.
Mondal, S.K., Wang, Y., Zhai, J., Su, B., Jiang, S., Huang, J., Gao, M., 2022. Projected urban exposure to extreme precipitation over South Asia. Sci. Total Environ. 822, 153664.
Mosavi, A., Ozturk, P., Chau, K.-W., 2018. Flood prediction using machine learning models: literature review. Water 10 (11), 1536.
Munna, G.M., Alam, M.J.B., Uddin, M.M., Islam, N., Orthee, A.A., Hasan, K., 2021. Runoff prediction of Surma basin by curve number (CN) method using ARC-GIS and HEC-RAS. Environ. Sustain. Indic. 100129.
Naghibi, S.A., Vafakhah, M., Hashemi, H., Pradhan, B., Alavi, S.J., 2020. Water resources management through flood spreading project suitability mapping using frequency ratio, k-nearest neighbours, and random forest algorithms. Nat. Resour. Res. 29, 1915–1933.
Naikoo, M.W., Talukdar, S., Das, T., Rahman, A., 2022. Identification of homogenous rainfall regions with trend analysis using fuzzy logic and clustering approach coupled with advanced trend analysis techniques in Mumbai city. Urban Clim. 46, 101306.
Natekin, A., Knoll, A., 2013. Gradient boosting machines, a tutorial. Front. Neurorobot. 7, 21.
Netzel, L.M., Heldt, S., Engler, S., Denecke, M., 2021. The importance of public risk perception for the effective management of pluvial floods in urban areas: a case study from Germany. J. Flood Risk Manag. 14 (2), e12688.
Ohba, M., Sugimoto, S., 2019. Differences in climate change impacts between weather patterns: possible effects on spatial heterogeneous changes in future extreme rainfall. Clim. Dyn. 52 (7), 4177–4191.
Paul, G.C., Saha, S., Hembram, T.K., 2019. Application of the GIS-based probabilistic models for mapping the flood susceptibility in Bansloi sub-basin of Ganga-Bhagirathi river and their comparison. Remote Sens. Earth Syst. Sci. 2, 120–146.
Pedregosa, F., Varoquaux, G., Gramfort, A., Michel, V., Thirion, B., Grisel, O., Dubourg, V., 2011. Scikit-learn: machine learning in Python. J. Mach. Learn. Res. 12, 2825–2830.
Pervin, I.A., Rahman, S.M.M., Nepal, M., Haque, A.K.E., Karim, H., Dhakal, G., 2020. Adapting to urban flooding: a case of two cities in South Asia. Water Policy 22 (S1), 162–188.
Pittman, S.J., Brown, K.A., 2011. Multi-scale approach for predicting fish species distributions across coral reef seascapes. PLoS One 6 (5), e20583.
Priyambodoho, B.A., Kure, S., Yagi, R., Januriyadi, N.F., 2021. Flood inundation simulations based on GSMaP satellite rainfall data in Jakarta, Indonesia. Prog. Earth Planet. Sci. 8 (1), 1–17.
Prokhorenkova, L., Gusev, G., Vorobev, A., Dorogush, A.V., Gulin, A., 2017. CatBoost: unbiased boosting with categorical features. In: arXiv Preprint arXiv: 1706.09516.
Rasool, U., Chen, J., Muhammad, S., Siddique, J., Venkatramanan, S., Sabarathinam, C., Rasool, M.A., 2020. Geoinformatics and geophysical survey-based estimation of best groundwater potential sites through surface and subsurface indicators. Arab. J. Geosci. 13 (15), 1–17.
Razavi-Termeh, S.V., Sadeghi-Niaraki, A., Choi, S.-M., 2019. Groundwater potential mapping using an integrated ensemble of three bivariate statistical models with random forest and logistic model tree models. Water 11 (8), 1596.
Rodriguez-Galiano, V., Chica-Olmo, M., Abarca-Hernandez, F., Atkinson, P.M., Jeganathan, C., 2012. Random forest classification of Mediterranean land cover using multi-seasonal imagery and multi-seasonal texture. Remote Sens. Environ. 121, 93–107.

Rokach, L., 2010. Ensemble-based classifiers. Artif. Intell. Rev. 33, 1–39.
Roy, P., Pal, S.C., Chakrabortty, R., Chowdhuri, I., Malik, S., Das, B., 2020. Threats of climate and land use change on future flood susceptibility. J. Clean. Prod. 272, 122757.
Rufo, D.D., Debelee, T.G., Ibenthal, A., Negera, W.G., 2021. Diagnosis of diabetes mellitus using gradient boosting machine (LightGBM). Diagnostics 11 (9), 1714.
Sandink, D., Robinson, B., 2022. Wastewater system inflow/infiltration and residential pluvial flood damage mitigation in Canada. Water 14 (11), 1716.
Sangati, M., Borga, M., 2009. Influence of rainfall spatial resolution on flash flood modelling. Nat. Hazards Earth Syst. Sci. 9 (2), 575–584.
Sathish, S., Chanu, S., Sadath, R., Elango, L., 2022. Impacts of regional climate model projected rainfall, sea level rise, and urbanization on a coastal aquifer. Environ. Sci. Pollut. Res. 29 (22), 33305–33322.
Shafizadeh-Moghadam, H., Valavi, R., Shahabi, H., Chapi, K., Shirzadi, A., 2018. Novel forecasting approaches using combination of machine learning and statistical models for flood susceptibility mapping. J. Environ. Manag. 217, 1–11.
Shen, C., Laloy, E., Elshorbagy, A., Albert, A., Bales, J., Chang, F.-J., Fang, Z., 2018. HESS opinions: incubating deep-learning-powered hydrologic science advances as a community. Hydrol. Earth Syst. Sci. 22 (11), 5639–5656.
Soni, J., Ansari, U., Sharma, D., Soni, S., 2011. Predictive data mining for medical diagnosis: an overview of heart disease prediction. Int. J. Comput. Appl. 17 (8), 43–48.
Spekkers, M., Kok, M., Clemens, F., Ten Veldhuis, J., 2013. A statistical analysis of insurance damage claims related to rainfall extremes. Hydrol. Earth Syst. Sci. 17 (3), 913–922.
Statistics, P. B. O, 2017. Government of Pakistan.
Stine, R.A., 1995. Graphical interpretation of variance inflation factors. Am. Stat. 49 (1), 53–56.
Tayfur, G., Singh, V.P., Moramarco, T., Barbetta, S., 2018. Flood hydrograph prediction using machine learning methods. Water 10 (8), 968.
Tehrany, M.S., Pradhan, B., Mansor, S., Ahmad, N., 2015. Flood susceptibility assessment using GIS-based support vector machine model with different kernel types. Catena 125, 91–101.
Ten Veldhuis, J., Harder, R., Loog, M., 2013. Automatic classification of municipal call data to support quantitative risk analysis of urban drainage systems. Struct. Infrastruct. Eng. 9 (2), 141–150.
Teng, J., Jakeman, A.J., Vaze, J., Croke, B.F., Dutta, D., Kim, S., 2017. Flood inundation modelling: a review of methods, recent advances and uncertainty analysis. Environ. Model. Softw. 90, 201–216.
Thanh Son, N., Thi Thu Trang, N., Bui, X.T., Thi Da, C., 2022. Remote sensing and GIS for urbanization and flood risk assessment in Phnom Penh, Cambodia. Geocarto Int. 37 (22), 6625–6642.
Torrence, C., Compo, G.P., 1998. A practical guide to wavelet analysis. Bull. Am. Meteorol. Soc. 79 (1), 61–78.
Urbanowicz, R.J., Meeker, M., La Cava, W., Olson, R.S., Moore, J.H., 2018. Relief-based feature selection: introduction and review. J. Biomed. Inform. 85, 189–203.
Ushio, T., Sasashige, K., Kubota, T., Shige, S., Okamoto, K.I., Aonashi, K., Kachi, M., 2009. A Kalman Filter Approach to the Global Satellite Mapping of Precipitation (GSMaP) from Combined Passive Microwave and Infrared Radiometric Data. 気象集誌. 第 2 輯, 87, pp. 137–151.
Venkatasubramaniam, A., Wolfson, J., Mitchell, N., Barnes, T., JaKa, M., French, S., 2017. Decision trees in epidemiological research. Emerg. Themes Epidemiol. 14 (1), 1–12.
Wu, X., Liu, Q., Huang, C., Li, H., 2022. Mapping heat-health vulnerability based on remote sensing: a case study in Karachi. Remote Sens. 14 (7), 1590.
Wu, Z., Bhattacharya, B., Xie, P., Zevenbergen, C., 2023. Improving flash flood forecasting using a frequentist approach to identify rainfall thresholds for flash flood occurrence. Stoch. Env. Res. Risk A. 37 (1), 429–440.
Xue, X., Zhang, K., Tan, K.C., Feng, L., Wang, J., Chen, G., Yao, J., 2022. Affine transformation-enhanced multifactorial optimization for heterogeneous problems. IEEE Trans. Cybern. 52 (7), 6217–6231. https://doi.org/10.1109/TCYB.2020.3036393.
Yan, Y., Zhang, N., Zhang, H., 2023. Applications of advanced technologies in the development of urban flood models. Water 15 (4), 622.
Yang, T.-H., Hwang, G.-D., Tsai, C.-C., Ho, J.-Y., 2016. Using rainfall thresholds and ensemble precipitation forecasts to issue and improve urban inundation alerts. Hydrol. Earth Syst. Sci. 20 (12), 4731–4745.
Yin, H., Wu, Q., Yin, S., Dong, S., Dai, Z., Soltanian, M.R., 2023. Predicting mine water inrush accidents based on water level anomalies of borehole groups using long short-term memory and isolation forest. J. Hydrol. 616, 128813.
Yoshimoto, S., Amarnath, G., 2017. Applications of satellite-based rainfall estimates in flood inundation modeling—a case study in Mundeni Aru River Basin, Sri Lanka. Remote Sens. 9 (10), 998.
Youssef, A.M., Pourghasemi, H.R., Pourtaghi, Z.S., Al-Katheeri, M.M., 2016. Landslide susceptibility mapping using random forest, boosted regression tree, classification and regression tree, and general linear models and comparison of their performance at Wadi Tayyah Basin, Asir region, Saudi Arabia. Landslides 13 (5), 839–856.
Yu, M., Liu, Y., Miao, S., 2020. Impact of urbanization on rainfall of different strengths in the Beijing area. Theor. Appl. Climatol. 139, 1097–1110.
Yuan, F., Mobley, W., Farahmand, H., Xu, Y., Blessing, R., Dong, S., Brody, S.D., 2021. Predicting road flooding risk with machine learning approaches using crowdsourced reports and fine-grained traffic data. In: arXiv Preprint arXiv:2108.13265.
Zhang, N., 2007. Scale issues in ecology: upscaling. Acta Ecol. Sin. 27 (10), 4252–4266.
Zou, X., Ren, F., 2015. Changes in regional heavy rainfall events in China during 1961–2012. Adv. Atmos. Sci. 32, 704–714.